

Fibrous Viscoelastic Extracellular Matrix Assists Precise Neuronal Connectivity

Ruipei Xie, Xiaoyu Yu, Ting Cao, Chen Yang, Yiyu Zhang, Xiaochen Wang, Yi-Jun Liu, Shumin Duan, Fangfu Ye,* and Qihui Fan*

Synapse formation in complex neuronal network is a pivotal process for normal functioning of nervous system. Although intense research has been conducted, how neurons and axons are guided toward the target remains largely unclear. In traditional opinions, axons are directed through chemotaxis, while recently mechanotaxis has been brought up as a potential complementary mechanism, as it can provide delicately controlled signals in addition to the random diffusive chemical cues. To further explore the path-finding mechanism, a quasi-3D in vitro model for neuronal cells is constructed by integrating hydrogel collagen I as extracellular matrix (ECM), and primary mouse cortical neurons and PC12 cells are tested. It is strikingly found out that axons and neuronal cells can be precisely guided toward target neurites via ECM. By developing a label-free traction force microscopy technique, the force networks among neurons are presented, validating that the fibrous matrix-transmitted paratensile signals can assist the axon pathfinding. This precise axon guidance is related to the activation of mechanosensitive ion channels, calcium signaling, and probably the following F-actin assembly. This mechanism can potentially assist developing clinical applications and designing biomaterials in near future.

During early development, the neuronal cells migrate or extend axons along well-defined pathways^[1–2] to form synaptic connections among adjacent cells. However, as one of the most important fundamental questions in neuroscience, it is still poorly understood that how neuronal cells are precisely guided to the proper target cells for synaptic formation.^[3–6] The current studies of axon pathfinding are mostly based on chemotaxis induced by attractive or repulsive guidance molecules.^[7–11] However, the transmission of chemical signals is relatively diffusive, which is limited in providing precise spatial resolution,^[12] especially for recognizing single cells or even single neurites with sizes of micrometer to sub-micrometer in complex microenvironment. Therefore, it is important to find out that if there is other complementary mechanism, which can assist this delicate pathfinding task.^[13–14]

Growing evidences imply that physical properties of extracellular matrix (ECM), such as matrix stiffness,^[15–16] mechanical

stimulation,^[17–19] substrate morphology,^[20] are essential in neuronal cell guidance. In previous studies on epithelial cells or fibroblasts, it was found that ECM can assist the transmission of paratensile signaling^[21–24] for remote communication

1. Introduction

The normal functioning of nervous system depends on the proper and efficient formation of synapse and neuronal network.

R. Xie, X. Yu, T. Cao, C. Yang, Y. Zhang, X. Wang, F. Ye, Q. Fan
Beijing National Laboratory for Condensed Matter Physics
Institute of Physics
Chinese Academy of Sciences
Beijing 100190, China
E-mail: fye@iphy.ac.cn; fanqh@iphy.ac.cn

R. Xie, Y. Zhang, F. Ye
School of Physical Sciences
University of Chinese Academy of Sciences
100049 Beijing, China

X. Yu, C. Yang
School of Mechanical Engineering & Automation
Beihang University
Beijing 100191, China

T. Cao, X. Wang, F. Ye
Oujiang Laboratory (Zhejiang Lab for Regenerative Medicine, Vision and Brain Health), Wenzhou Institute
University of Chinese Academy of Sciences
Wenzhou, Zhejiang 325000, China

Y.-J. Liu, S. Duan
Department of Neurobiology, NHC and CAMS Key Laboratory of Medical Neurobiology, School of Brain Science and Brain Medicine, and the MOE Frontier Science Center for Brain Research and Brain-Machine Integration
Zhejiang University School of Medicine
Hangzhou 310058, China

S. Duan
Mental Health Center
Zhejiang University School of Medicine
Hangzhou, Zhejiang 310058, China

 The ORCID identification number(s) for the author(s) of this article can be found under <https://doi.org/10.1002/adfm.202301926>

DOI: 10.1002/adfm.202301926

among cells.^[25–26] Besides, neurites have been demonstrated to extend along the fibrous materials, such as nanofibers,^[27] and the synapse formation is enhanced with the support of ECM hydrogels.^[28–29] However, it is still unknown that how these ECM materials play roles in path-finding of neuronal cells for synapse formation during development or regeneration of neuronal system.

To further explore the ECM materials related axon-pathfinding mechanism, we constructed a quasi-3D in vitro system with collagen hydrogel as ECM, and seeded primary mouse cortical neurons or PC12 cells, onto the hydrogel, mimicking an in vivo-like microenvironment. The analysis of cell dynamic is applied under our improved label-free traction force microscopy (TFM), which uses microstructures of ECM as tracing markers to calculate the deformation field formed by cell with estimated collagen stiffness.^[30–31] This improved TFM technique well reserves the cell motilities and mechanical responses during long time tracking processes, by avoiding the fluorescent labeling and extra phototoxicity on cells. Meanwhile, the external mechanical stimuli on collagen hydrogel, which is then transmitted to the nearby cells, are mimicked by micromanipulation systems with customized controlling program.

In the integrated quasi-3D system, it is revealed that neuronal cells can precisely communicate with the target cell, and axons are precisely guided for synapse formation via fibrous matrix-transmitted rhythmic paratensile signaling. Further analysis confirms that this hydrogel-assisted axon path-finding mechanism is related to the activation of mechanosensitive ion channels and the downstream local calcium signals, which can cause the F-actin polymerization and induce axon extensions along the stimulated direction.^[11] This novel mechanism advances our understanding of how the ECM materials assisted transmitting mechanical signals to precisely guide neuronal cells migration and axon extensions, which eventually aid the synapse formation in nervous system. The in vitro models with integrated hydrogel materials for transmission of mechanical signals among neurons can also function in neuron regenerative studies, thus potentially inspire new clinical applications, and guide the design of biomedical materials.^[32–33]

2. Results

2.1. Precise Guidance of Neuronal Cells on Collagen ECM

Precise guidance of neuronal cells on collagen ECM. A quasi-3D in vitro model is constructed by distributing individual neuronal cells (differentiated PC12 cells and primary mouse cortical neurons) onto type I collagen hydrogel (Figure 1a,b; and Figures S1 and S2a, Supporting Information) to mimic in vivo-like microenvironment. Collagen I hydrogel is a major ECM component in vivo, which has fibrous microstructures with nonlinear viscoelastic properties.^[34] With ECM as substrate, neuronal cells reconstructed surrounding collagen fibers to form bundles, which bridged between the neighboring active cells. The bridged neuronal cells presented strongly correlated migration, and their axon extensions directly approached to each other along the microfiber bridges within a range of around 100 μm , realizing precise cell guidance for synaptic formation (Figure 1a,b). In contrast, if cells were cultured on substrate of solid culture dish, lack-

ing of the ECM-transmitted paratensile signaling, they would not sense each other or form strong correlation remotely, thus presenting a random migration (Figure 1c,d).

The detailed cell pathfinding strategy via paratensile signaling is illustrated in Figure 1a; and Figure S1a (Supporting Information). Initially, cells extend multiple transient protrusions in random directions, pulling the collagen fibers toward the cell center, and reconstructing these microfibers parallel to the cell protrusions (Figure 1a, white arrow). If both of neighboring neuronal cells actively pull the collagen fibers toward themselves, the collagen fibers between the two cells are stretched and gradually remodeled into long and thick bridged fiber bundles (Figure 1a, blue arrow, tested with PC12 cells; and similar results with primary cortical neurons in Figure S2a, Supporting Information). Then cells continue to extend axons and migrate toward each other along the bridged fiber bundles, until connected with the other cell. After tight connection, calcium wave can sequentially transmit from one cell to another (Figure S3 and Movie S1, Supporting Information), indicating that these precisely connected cells can form effective communication. Neuronal cells with weak contractile activity cannot dramatically reconstruct the surrounding matrix as fast as other active cells, and thus, cannot effectively communicate with other cells via paratensile signaling (Figure 1a, blue star).

To investigate the formation of collagen fiber bundles between neuronal cells, an improved label-free TFM technique is applied to study the collagen strain during cell migration and axons extension. The microstructures of ECM fibers, which are traced under inverted microscopy even in bright field, are used as reference marks for particle image velocimetry (PIV, one of the TFM tracing algorithm),^[35–36] to analyze the dynamic change of the ECM microstructures and to obtain the cell-caused ECM deformation. The deformation field shows that neuronal cells constantly contract the nearby collagen as they extended the axons, causing a significant collagen deformation (Figure 1e). The collagen was contracted toward the intercellular region and was pulled toward the adjacent cell, thus forming a region of steep color changes between cells in the map of vector direction (region marked by white dashed box, Figure 1f). Here, we propose divergence diagram (Divergence $\theta = \partial\mu/\partial x + \partial\nu/\partial y$, as illustrated in the Experimental Section) to further analyze collagen fiber densification (Figure 1g). The divergence results clearly show that collagen fibers near the active cells were dramatically contracted and stretched to form dense fiber bundles (red), bridging with nearby cells for precise and efficient paratensile signaling transmission. The primary mouse cortical neurons are also tested in the quasi-3D model, and the analysis of the mechanical signals verified the similar results (Figure S2b–d, Supporting Information).

Based on precise synapse formation results in cell-pair studies, the formation of neuronal network is further studied by applying a group of cells in the model. The neuronal cells on collagen rapidly self-assembled into a well-organized network containing almost all the cells within 3 h (PC12 cells in Figure 1h; and Figure S4a and Movie S2 (Supporting Information); primary cortical neurons in Figure S5a,c, Supporting Information), while cells on solid culture dish remained discrete, with anisotropic and uncorrelated orientations (PC12 cells in Figure 1i; and Figure S4b and Movie S3 (Supporting Information); primary cortical neurons in Figure S5b, Supporting Information).

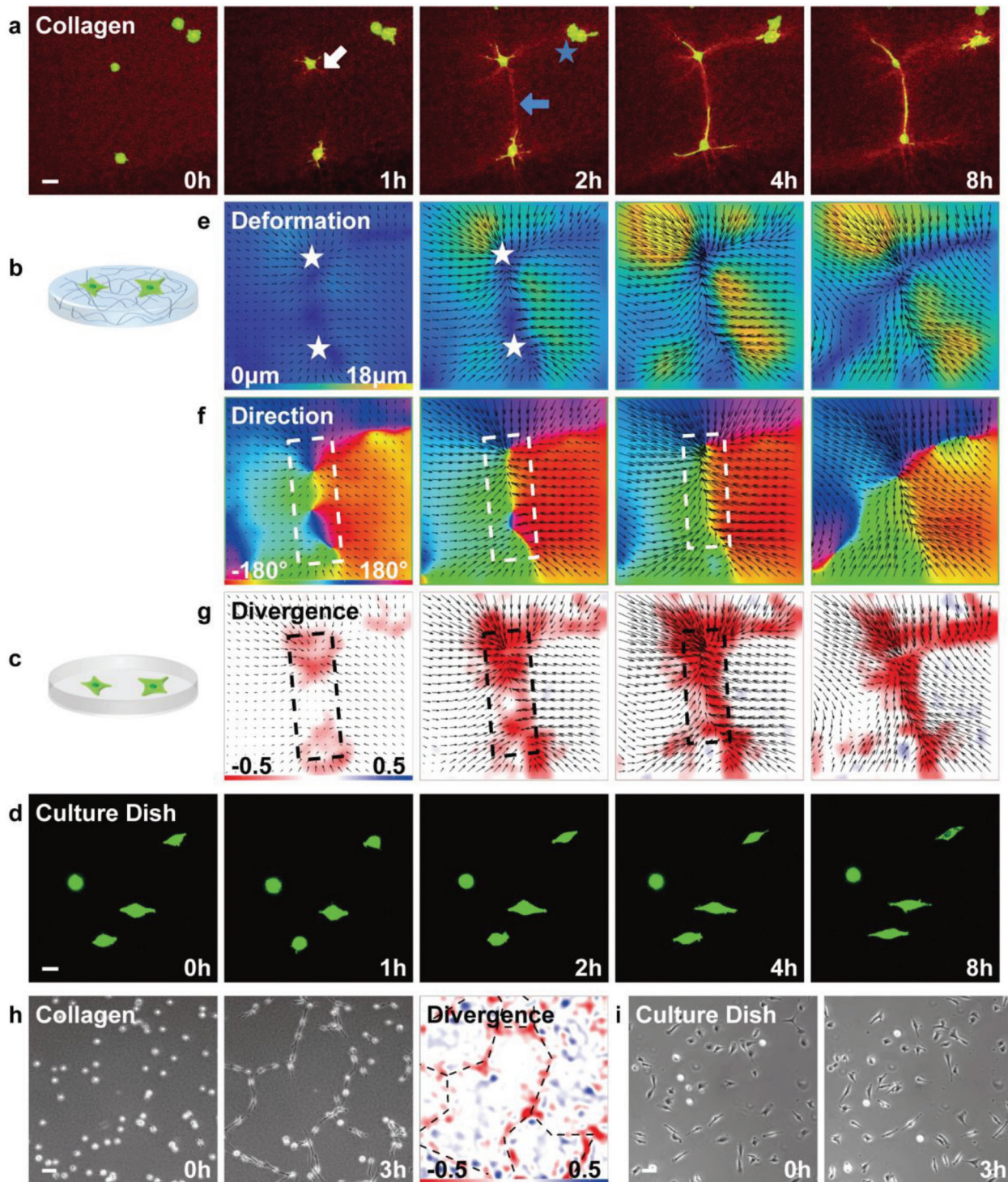


Figure 1. PC12 cells migrate and extend axon towards each other via collagen-fiber transmitted paratensile signals, enabling precise cell connections for synapse formation. a) A representative pair of cells (green) exhibit strongly correlated migration and axon extending dynamics, and have remodeled nearby collagen fiber bundles (red). The white arrow indicates the collagen fibers that are initially and randomly reconstructed. The blue arrow indicates the collagen fibers between the cells undergo significantly reorganization. The blue star marks a cell, which does not significantly contract and reorganize the surrounding collagen, and thus, cannot form enough communication with other cells and could not migrate toward them instantly. Scale bar is 20 μm . b,c) Schematic of experimental systems for quasi-3D a) and 2D d) in vitro cell cultures. d) Cells cultured on top of solid culture dish cannot form strong correlated migration or be reoriented to form neuronal connections remotely. Scale bar is 20 μm . e–g) The corresponding deformation field e), resulting vector direction f), and divergence diagram g) of collagen obtained by TFM at different time. The black arrows indicate the directions of the local displacements. h,i) Time-lapse diagrams of rapid cell self-assembly on collagen h) and on culture dish i). The resulting divergence diagram during cell network formation, with the cell network outline marked with black dotted lines. Scale bar is 100 μm .

In order to exclude the influence of cell-induced chemical signal gradients, we introduced microflows in the collagen culture system to eliminate chemical gradients and characterized the flows by adding tracer particles in the fluid (Figure S4e, Supporting Information). In order to avoid the deposition of tracer particles affecting cell migration behavior, no tracer particles were added in the cell experiment. Under the action of microflows, the neuronal cells on collagen can still self-assembled into a well-organized network (Figure S4c, Supporting Information). To eliminate the influence of chemical ligands of ECM, collagen was modified on the surface of culture dish, and the neuronal cells remained discrete distribution on the modified surface (Figure S4d, Supporting Information). Neuronal cells embedded in ECM showed that neuronal cells still exhibit precise connection in the 3D system (Figure S6c, Supporting Information).

The divergence data from the TFM (Figure 1h; and Figure S5a, Divergence, Supporting Information) and the confocal image of collagen (in quasi-3D system, Figure S6a (Supporting Information); in 3D system, with neuronal cells embedded in collagen gel, Figure S6b, Supporting Information) both confirmed that densified collagen fiber bundles were formed among cells, and collagen displayed a nearly identical network structure synchronously with the neuronal network.

2.2. Characterizations of Directional Neuronal Migration

Except for the guidance of axon extensions, the neuronal cells' migration is found to be strongly correlated with the mechanical communication among cells. The migration dynamics of PC12 cells are quantified by analyzing time-lapse cell trajectories (Figure 2a; and Figure S7, Supporting Information). The normalized cell-pair distances (CD_i/CD_0) decrease rapidly as a function of time in the quasi-3D system, while the distances between the cells on culture dish substrate fluctuate randomly (Figure 2b,c). The results clearly show that neuronal cells can be attracted to neighboring target cells via paratensile signals transmitted through collagen gel, even when there is a long distance between them (150–400 μm) without obvious collagen fiber bundles formed yet. In contrast, solid substrate could not transmit these signals to provide effective communications. These results are also supported by analysis of the cell-pair migration linearity, as quantified by the ratio of the change in distance between cells to the total migration distance of cells ($(CD_0 - CD_i)/(D_{1i} + D_{2i})$), on both collagen and solid substrates (Figure 2d,e).

The efficiency of neuronal cell migration is investigated based on cell trajectory analysis, i.e., mean squared displacement (MSD), average speed, directional ratio, and autocorrelation coefficient (Figure 2g–k).^[37] Representative trajectories clearly show that cells on collagen have longer migration distances and more distinct directions (Figure 2f; and Figure S8, Supporting Information). The slope α of MSD ($\langle (d_i)^2 \rangle$) of cells on collagen is 1.80 ± 0.01 (Figure 2g), and that of cells on culture dish is 1.49 ± 0.01 . Both α values are larger than 1, indicating that the migration modes of neuronal cells are super-diffusive on both types of substrates. Moreover, the persistence of cell migration on collagen is much higher than that on culture dish due to the larger α value. The average speed of cells on collagen is significantly higher than that on culture dish (Figure 2i). The directional ra-

tio (d_i/D_i) of cells on collagen is also significantly higher than that on culture dish (Figure 2h,j), indicating that the cells on collagen are much more directional persistent. However, there was no significant difference in the autocorrelation co-efficiency ($\langle \cos(\theta) \rangle = \langle (\mathbf{S}_{i-1} \cdot \mathbf{S}_i) / |\mathbf{S}_{i-1}| |\mathbf{S}_i| \rangle$) between the two groups (Figure 2k), implying that the correlation of the instantaneous movement of cells on the two substrates was similar.

2.3. Tensile Signaling of Neuronal Cells and Its Innate Rhythmicity

The physical mechanism of the paratensile signaling is further studied by characterizing the dynamic deformation magnitude caused by single neuronal cell. The deformation and stress field^[38–39] analyzing results show that neuronal cells started to spread and reconstruct the surrounding collagen fibers within 0.5 h after cell seeding (Figure 3a,b; and Figure S9, Supporting Information). The obtained stress magnitude is within the range of promoting neurite growth when neurons are stretched directly by external mechanical force.^[40–41] It is also demonstrated that maximum collagen strain happened along the polarized major cell axons, and the strain was increased with time. The deformation fields evolved with time are quantified by orienting the fields along the long axis of cells ($\theta = 0^\circ$), with cell centroid as origin point (Figure 3c–e). The average collagen deformation shows a nonuniform field created by bipolar-contracting cells, and the ratio of axial to transversal deformation exceeds 2.7 (Figure 3c). The deformation curve of collagen presents the average strain values along with the distances away from the cell centroids at different time points (Figure 3d). The curve clearly shows that the collagen at distances of more than 150 μm away from cell still have significant deformation, indicating that collagen could transmit the local strain to the distance far beyond cell size. The average deformation field demonstrates that the degree of local collagen strain increases with time, but the increment decreases gradually (Figure 3e). The collagen average deformation reaches to the plateau of around 8 μm at 4 h, which is probably due to the nonlinear viscoelastic property of collagen,^[34,42] i.e., collagen's young's modulus enhances with the increasing strain.

The TFM analyzed deformation fields also demonstrate how cells dynamically interacted with their collagen substrate. As shown in Figure 4a–c, during the neuronal cell's migration, the front protrusions (right) of the cell contracted the surrounding collagen gel, especially the collagen in front of cell, while the rear (left) of the cell relaxed the collagen and was retracted forward (right), then the soma migrated forward along with its attached collagen.

Considering that the collagen deformation field has polarity, which is mainly along the long axis of cell, the deformation value of collagen along the long axis (i.e., the u component of deformation, Figure 4c) was extracted by averaging the deformation value within 20 μm width (along transverse axis) region, to calculate the dynamic neuronal cell contraction force on collagen over time (Figure 4e,f). The positions of cell front and rear over time were marked in the figure with red and blue dashed lines, respectively. The cumulative deformation along the long axis over time (Figure 4e) shows that the front protrusions of the neuronal cell continuously contracting its surrounding

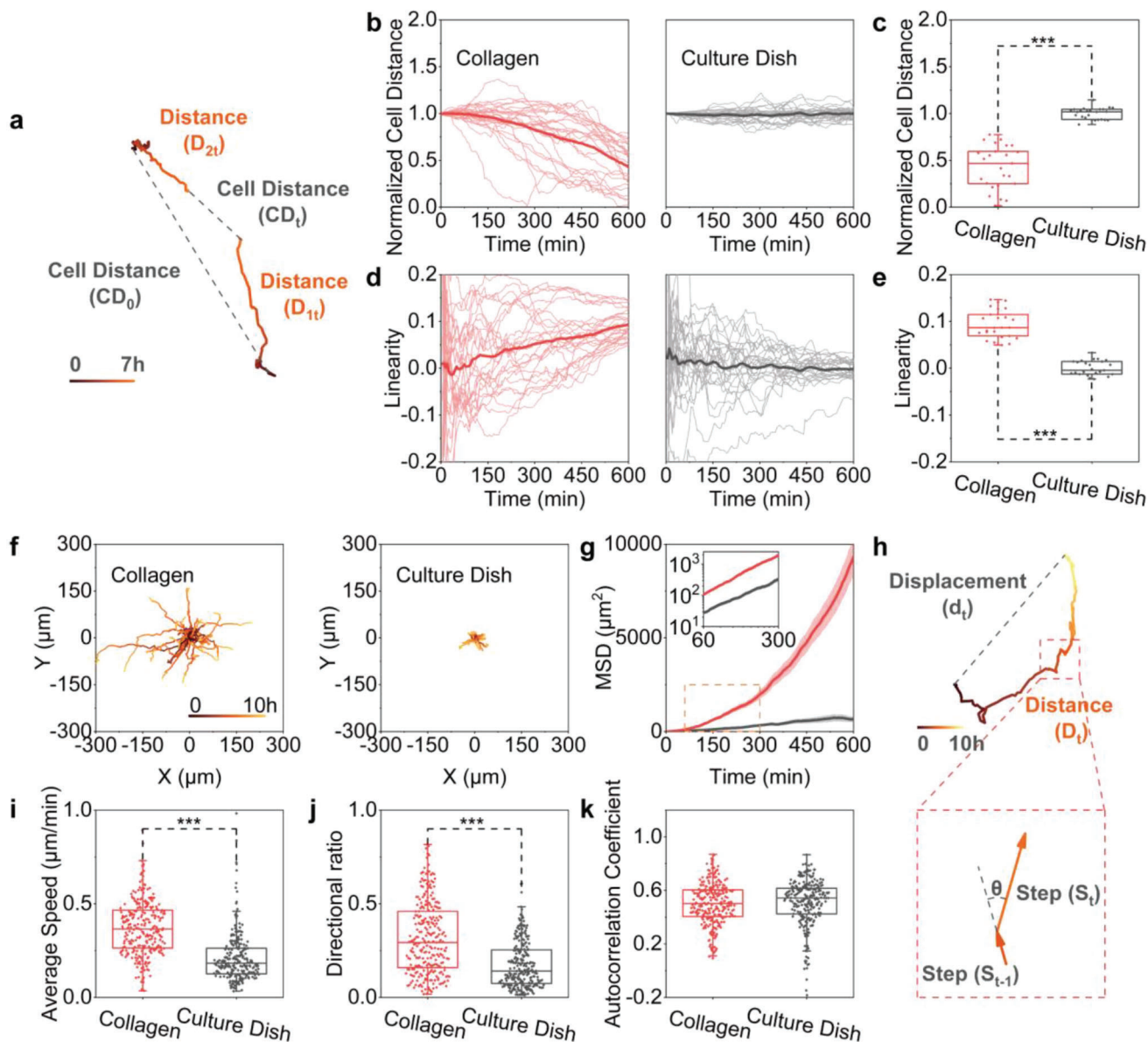


Figure 2. Characterizations of neuronal migration under paratensile signaling. a) Definition of cell distances for cell-pair trajectories. b–e) Dynamic changes of normalized distances between cells b) and linearity d) of cells on collagen (red) and culture dish (black) ($n = 25$), and statistic of normalized cell distances c) and linearity e) of cells on collagen and culture dish at final moments (600 min). Each dark thin line represents an independent experimental data, and the bright thick line represents the average of all data. f) Representative neuronal cell trajectories show the persistent migration on collagen and reciprocating random migration on solid substrate of culture dish. g) Mean square displacement (MSD) analysis of the cell migration on collagen (red, $n = 258$, $N = 3$) and culture dish (black, $n = 245$, $N = 3$). The inset is the log–log plot of MSD versus time, and the slope α is obtained by linear fitting. ($\alpha = 1.80 \pm 0.01$ for the cells on collagen and $\alpha = 1.49 \pm 0.01$ for the cells on culture dish). h) Schematic of cell migration characteristic parameters. i–k) Statistics of the average speed i), directional ratio j), and autocorrelation coefficient k) of cell migration on collagen and culture dish.

collagen, as the cell front sits on the boundary between the two colors. The collagen ahead of cell front position is pulled backward (blue region) and the collagen behind the cell front is pulled forward (red region), and the cumulative deformation increases over time. The divergence diagram (Figure 4d) presents the collagen near the front protrusion of the cell was contracted (red region) and the collagen near the rear protrusion of the cell was released (blue region), which further confirmed the above analysis.

The dynamic collagen deformation field further demonstrates that the ECM is periodically stretched by neuronal cells, indicating the innate rhythmic contraction of neuronal cell, which perfectly matches to the cyclic transmission mode of paratensile signaling.^[43] Not like the cumulative deformation with relatively stable directions, the transient deformation of collagen along the long axis of cell over time show that the collagen at the front and rear ends of the cell are alternately contracted and relaxed, but not in a constant contraction or relaxation mode (Figure 4f,g).

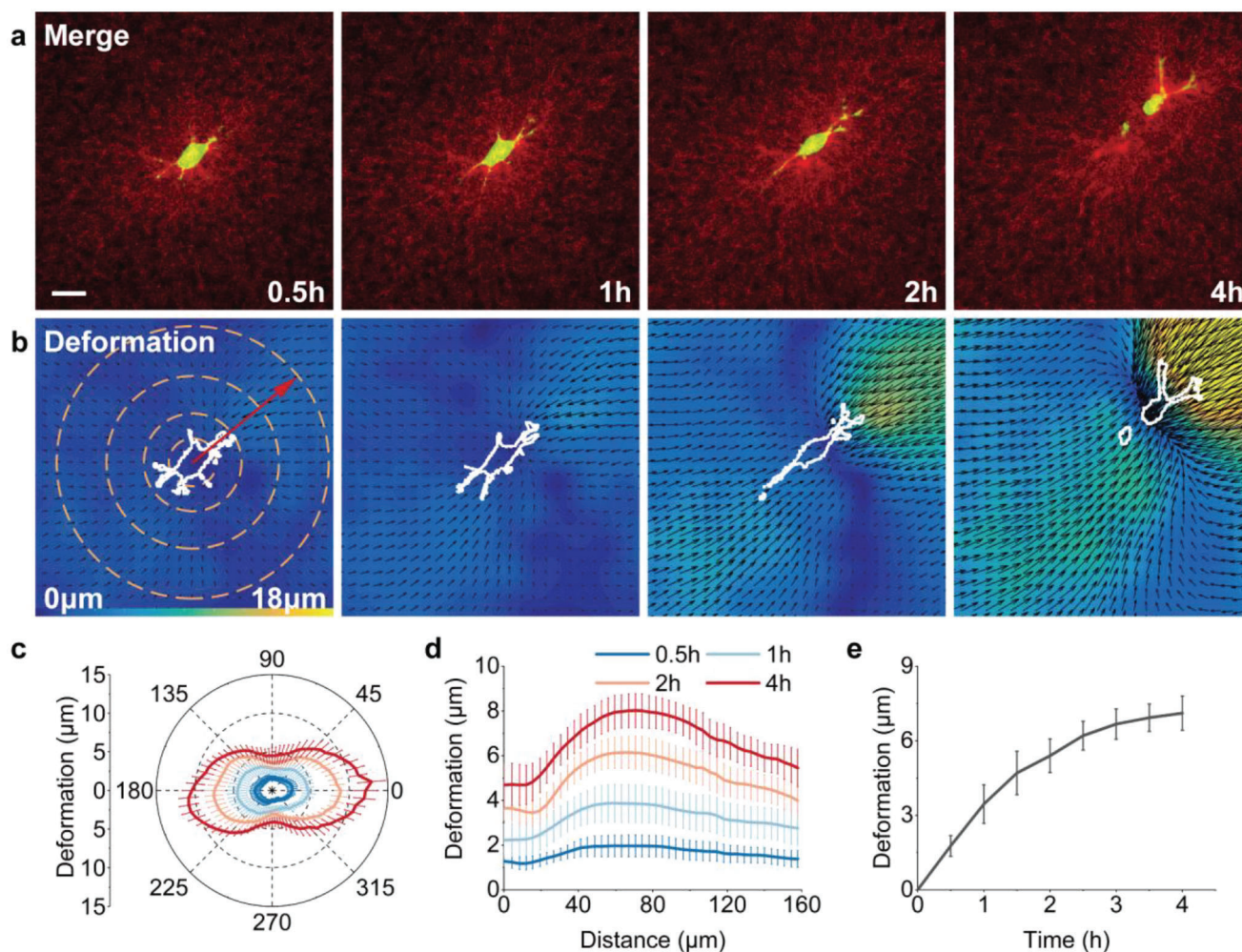


Figure 3. Characterizations of single neuronal cells' dynamic contraction. a, b) The morphology of cell (a, green) on collagen (a, red) and the corresponding deformation b) magnitude of collagen at different time. The deformation and stress values in the map correspond to the value in color bar, the superimposed black arrows mark the local displacement direction, and the cell outline is profiled with white dashed line. Scale bar is 20 μm . c–e) The average deformation field c), the corresponding deformation value versus distance along the long cell axis d), and the whole-cell averaged deformation value versus the time e) were quantified by orienting the fields along the long axis of cells ($\theta = 0^\circ$, as marked by the red arrow in b) left) with the cell centroid as the origin point ($N = 7$).

The cyclic neuronal cell stretching mode other than constant deformation mode contributes significantly to the paratensile signaling, because the tensile force transmission relies on repeatedly deformation application on collagen ECM, which has nonlinear visco-elasticity and relaxation properties. In another word, because the collagen fibers are not purely elastic, but also with the plastic property, if the deformation is only applied once, the tensile force transmitted through the collagen fiber will decrease rapidly.^[34] Thus, it requires repeated deformation caused by rhythmic cell contraction to maintain the effective tensile signaling via collagen matrix.

2.4. Cell Responses to Physically Applied Mechanical Signal

Collagen deformation was induced by physically applied mechanical stimuli, mimicking the adjacent cell's contraction force by a

micromanipulator-controlled micropipette with customized controlling program to realize static stretching and cyclic stretching (Figure 5a,b). Cyclic stretching is for mimicking the innate rhythmicity of neuronal cells' contraction force. Naturally, like the deformation field formed by cells (Figure 3b), micropipette stretching created a nonuniform deformation field on collagen gel (Figure 5c). Considering that stretching may damage collagen, we observed the changes of collagen morphology under different stretching amplitude and repeated times. If collagen was stretched for 60 times with a maximum deformation amplitude of 5 μm , no obvious damage was found on the surface of the collagen (Figure S10b, Supporting Information), confirmed that the stretch parameters used in our study were appropriate. However, when the maximum deformation amplitude was increased to 15 μm , prolonged stretching would cause damage on the collagen surface, which was located near the micropipette tip. In other words, there is a threshold limit on the deformation

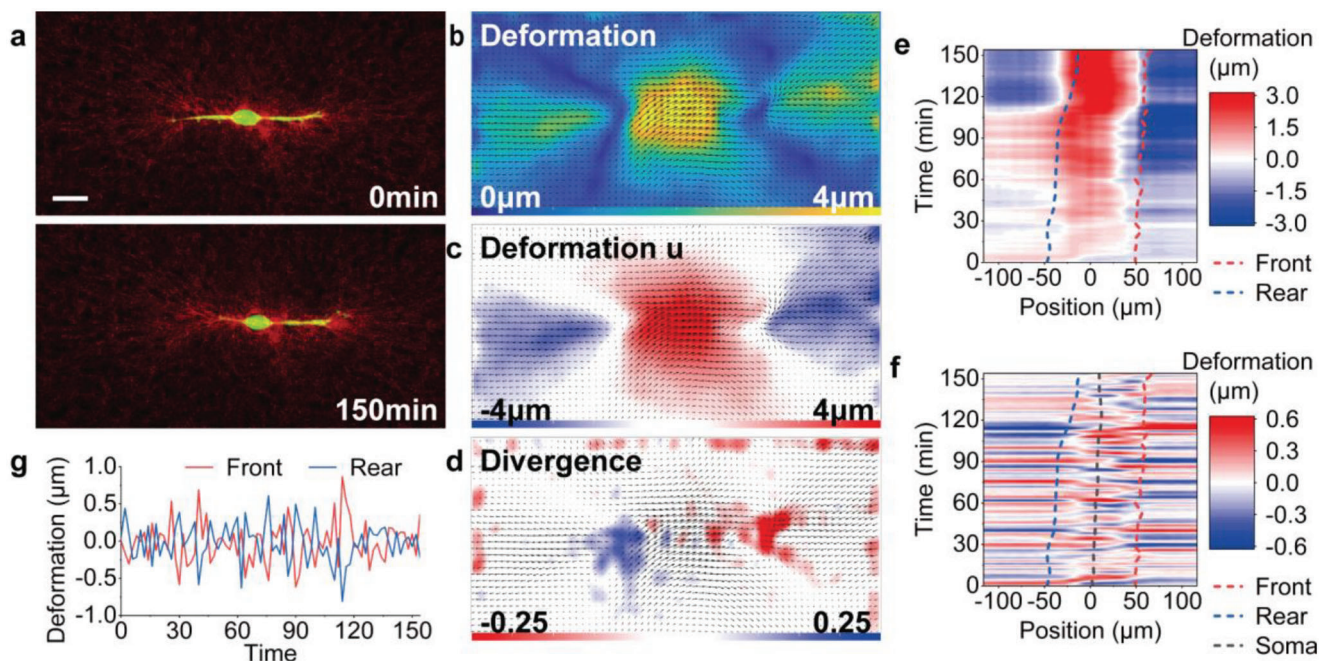


Figure 4. Intrinsic rhythmic contraction of neuronal cells. a–d) The morphology of cell and collagen at various time a), the corresponding deformation obtained by TFM b), the resulting deformation along the long axis of cell (u component) c), and divergence diagram d). Scale bar is $20\ \mu\text{m}$. e,f) The cumulative displacement e) and transient displacement f) of collagen at different distances from the cell centroid (origin point) along the long axis of cell over a 150 min period (red means the collagen shifted forward/to right, blue means the collagen shifted backward/to left). The front (red dashed line), soma (black dashed line), and rear (blue dashed line) positions of cell were marked. g) The dynamics of transient collagen displacement near the front (red) and rear (blue) of cell.

amplitude when the collagen is deformed using micropipette. It is exciting to find out that neuronal cells responded to the induced cyclic stretching by redirecting themselves and migrating to the micropipette tip as their response to another contracting cell (Figure 5d). The static stretching can induce cell redirection, but not as effectively as caused by cyclic stretching (Figure 5e). Due to the nonlinear viscoelastic property of collagen, the stretched collagen area has higher stiffness.^[34,42] Therefore, it is still consistent with durotaxis that cells migrate toward the stretched direction.

Various dynamic cell parameters are analyzed to quantitatively characterize the regulation of cell direction by physical stretching. The static stretching can slightly increase the speed, while the cell speed in cyclic stretching mode is similar to that of unstimulated cells (Figure 5g). This is probably due to repeated releasing-gel steps in cyclic stretching mode, which interferes the acceleration of cell speed. The normalized distance and the Angle between the direction of cell axon (Figure 5h–i) verify the mechano-response of neuronal cells by migrating or extending axon toward the micropipette-caused mechanical signals. The statistical results show that the cyclic stretching signal would guide neuronal cell more efficiently than static stretching signal.

2.5. Mechano-Transduction Mechanism for Neuron Pathfinding

In neuronal cells, how neurite can respond to matrix-transmitted mechanical signals and regulate cell migration is still largely unknown. However, mechanosensitive ion channels have been

often considered to participate in cell mechano-sensing pathways in recent years.^[32,44] One of mechanosensitive ion channels Piezo1 is also found to distribute on neuronal cells (Figure 6a; and Figure S5d, Supporting Information), as reported in previous studies.^[45–46] To verify the hypothesis and reveal the mechanism in detail, the mechanosensitive channels (Piezo and TRP families) are inhibited by a specific inhibitor GsMTx4. Then the degree of neuronal network formation is decreased, indicated by that part of cells are not included in the relatively weak network, but the morphology of cells is not significantly changed (Figure 6b; and Figure S11, Supporting Information). After inhibition, the autocorrelation coefficient of cell migration increased significantly (Figure 6d), while migration speed is maintained (Figure 6e; and Figure S12, Supporting Information). The results indicate that GsMTx4-treated neuronal cells move more randomly in the quasi-3D system, other than the strongly correlated migration for nontreated cells (Figure 6g,h; and Figure S13, Supporting Information). Therefore, it is revealed that mechanosensitive ion channels can influence the mechanical communication between cells, and reduce the ability of precise guidance for neuronal cell migration toward each other.

In order to eliminate the interference of nonphysical signals, we also applied the external mechanical stretching onto collagen near GsMTx4-treated cells, and the similar results are acquired (Figure 6i,j; and Figure S14, Supporting Information). After inhibitor treatment, the cell speeds are not changed in response to both static and cyclic stretching. However, the physical guidance on cells is dramatically impaired, indicating that the

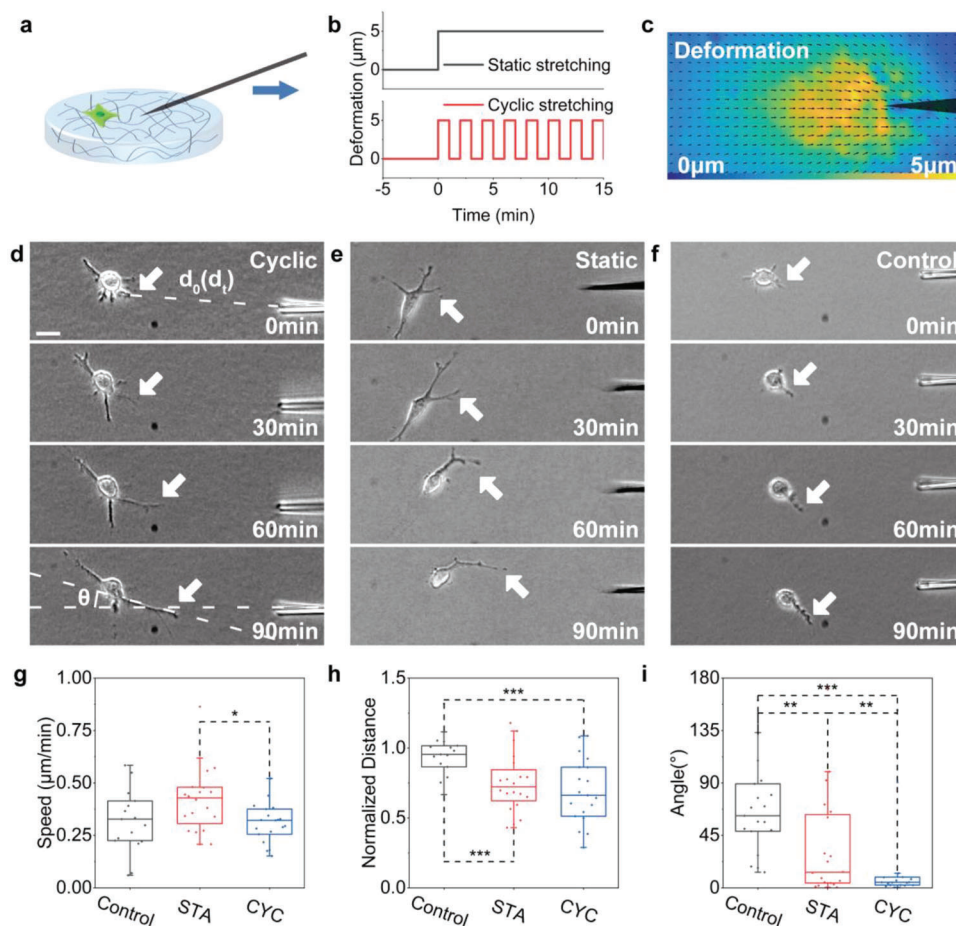


Figure 5. Cellular response to physically applied mechanical signals. a) Schematic of mechanical stimulation. b) The curve of collagen deformation with time under static stretching and cyclic stretching. c) The nonuniform deformation field produced by microneedle pulling. d–f) Time-lapse images of cyclic stretching stimulated cell d), static stretching stimulated cell e), and the cell in control group without stretching f). White arrows mark changes in the location of cell axons over time during stretching. Scale bar is 20 μm . g–i) Statistics of the average speed g), the normalized distance from cell axon to micropipette tip h), and the Angle between axon direction and stretching direction i) of cells under static stretching (STA), cyclic stretching (CYC), and no stretching in control group.

mechano-sensing ability of neuronal cells is strongly related to mechano-sensitive ion channels.

Moreover, it has been known that calcium signaling is strongly related to the activation of mechano-sensitive ion channels.^[47–48] Therefore, the downstream calcium signals are imaged by recording the fluorescence of cells, which are prestained with Calbryte-520 (5 μM , AAT). Ca^{2+} responses to the ECM-transmitted tensile signaling are analyzed under micropipette-induced artificial stretching on collagen. It is found that calcium intensity significantly increases at the specific axon immediately after sensing the mechanical signals (Figure 7a,b). After a transient response time (30.7 $\text{s} \pm 6.8$ s, Figure S15, Supporting Information), the calcium intensity at the axon front site reached to a peak (Figure 7b,c). Interestingly, we also find out that axon exhibit relatively high Ca^{2+} fluctuations when they are extending, while the Ca^{2+} fluctuations are relatively weak at stable or retracting states (Figure 7d). The frequency of calcium transients and average calcium intensity during protrusions extending are significantly higher than that during stalling or retracting (Figure 7e,f). If Ca^{2+} in the medium was removed by calcium chelator EGTA

(1 mM), the speeds (Figure 6e) and the strongly correlated cell migration (Figure 6g,h; and Figure S13, Supporting Information) are decreased significantly.

Also, Ca^{2+} plays an important role in neuronal axon growth and pathfinding^[40,49–50] by influencing actin polymerization to promote cell migration or elongation.^[7,11,51] Neuronal cells' F-actin expression is much higher at the axon front on collagen substrate, which is directly receiving the remote mechanical signals and approaching to the nearby cells (Figure 6a). This is also consistent with our hypothesis that tensile-signaling increased calcium can enhance the polymerization of F-actin at the stimulated axons. We further decreased the strength of actomyosin and polymerization of F-actin by applying the myosin II inhibitor Blebbistatin and actin polymerization inhibitor Latrunculin A, respectively. Inhibition of actomyosin resulted in a significant reduction in the formation of cell networks and collagen fiber bundles, while cells remained well spread (Figure 6b; and Figure S11, Supporting Information).

Therefore, our results indicate that ECM-transmitted tensile force signaling can induce a stress on the mechanosensitive ion

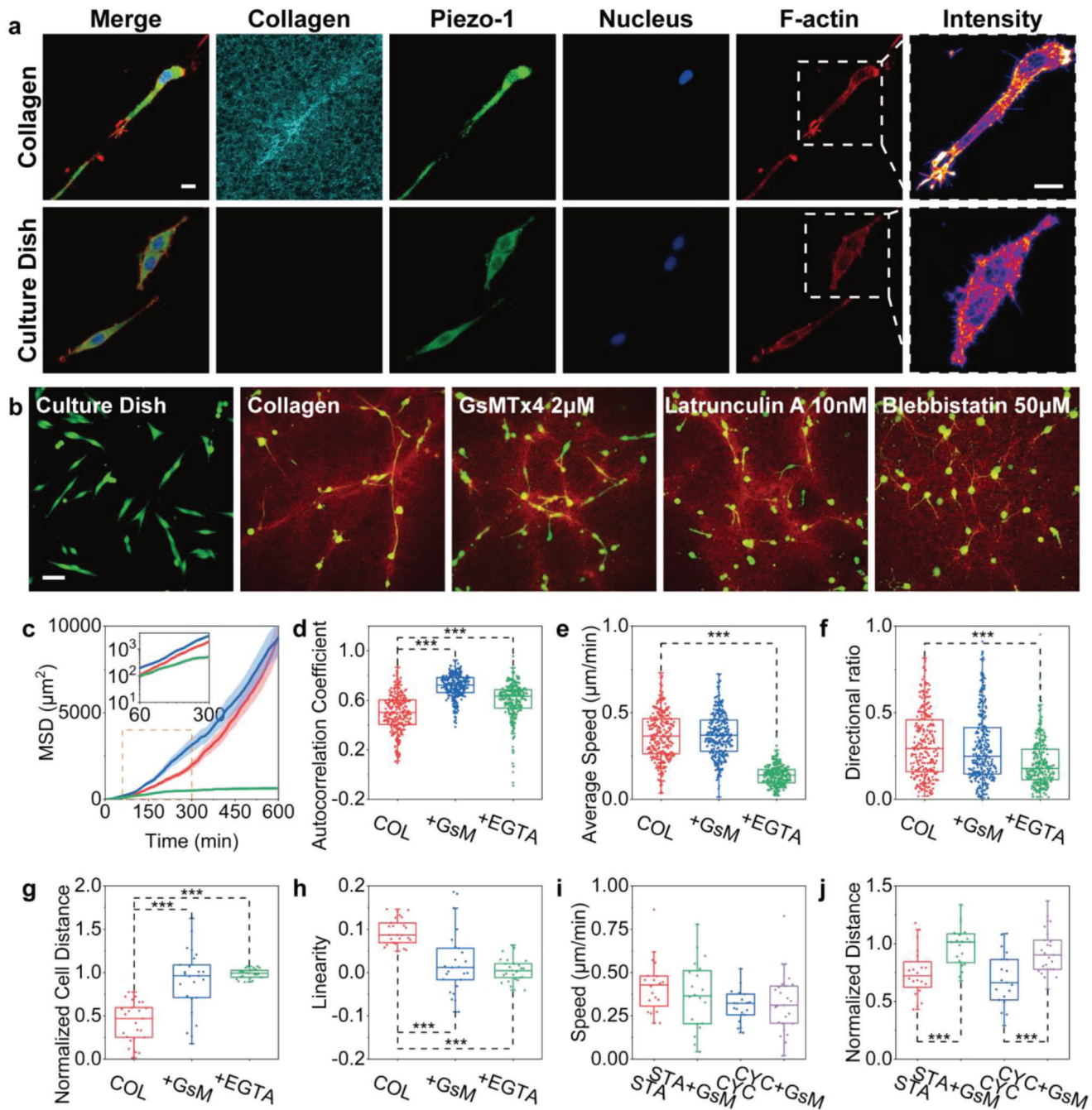


Figure 6. Explorations of the mechano-transduction mechanism. a) Immunofluorescence images of neuronal cells (PC12). Scale bar is 10 μm . b) Confocal images of neuronal networks (Green) on culture dish and collagen (Red) without any inhibitor treatment, and cells on collagen treated with 2 μM GsMTx4, 10 nM Latrunculin A, and 50 μM Blebbistatin, respectively. Scale bar is 50 μm . c) MSD analysis of the cell migration on collagen (red, $n = 258$, $N = 3$), on collagen and treated with 1 μM GsMTx4 (blue, $n = 290$, $N = 3$), and on collagen with 1 mM EGTA (green, $n = 245$, $N = 3$). The inset is the log-log plot of MSD versus time, and the slope α is obtained by linear fitting. ($\alpha = 1.80 \pm 0.01$ for cells on collagen, $\alpha = 1.84 \pm 0.01$ for cells on collagen with 1 μM GsMTx4, and $\alpha = 1.05 \pm 0.02$ for cells on collagen with 1 mM EGTA). d–f) Statistics of the average speed d), directional ratio e), and autocorrelation coefficient f) of cell migration on collagen (COL), on collagen with 1 μM GsMTx4 (+GsM), and on collagen with 1 mM EGTA (+EGTA). g, h) Statistics of normalized cell distance g) and linearity h) of cell pairs migration on collagen when cells were treated with 1 μM GsMTx4 (+GsM) or 1 mM EGTA (+EGTA). i, j) Statistics of the average speed i), and the normalized distance from cell axon to micropipette tip j) of cells.

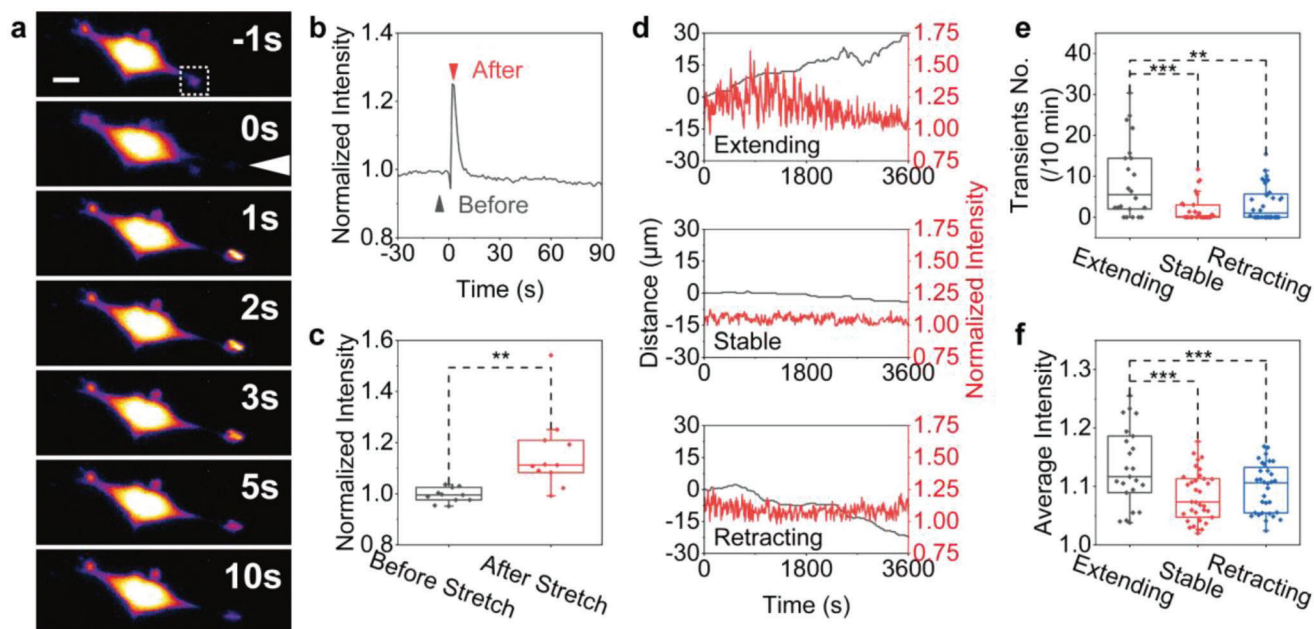


Figure 7. Calcium signaling and stimulated axon elongation analysis. a,b) Time-lapse calcium signaling of the responding axon (white dashed box) before and after the cell was stimulated by remotely applied force (a, the white arrow indicates micropipette position) and the curve of normalized calcium intensity at the responding axon front over time b). Scale bar is 10 μm . c) Normalized calcium intensity of the axon before and after stretching. d) Calcium activities (Normalized intensity, red) and the extended length (Distance, black) of the responding axon in the extending (up), stable (middle), and retracting (below) states, respectively. e,f) The mean numbers e) and average intensity f) of Ca^{2+} transients at the extending, stable, and retracting state of neuronal cell axon.

channels of axon front and activate the channels. The activation of ion channels will cause the enhancement of calcium signals at the local region of the stimulated axon, and the subsequent actin polymerization for extending of this axon,^[39–40] finally fulfilling precise guidance for axon pathfinding.

3. Conclusion

In this study, it is striking to find out that except for the chemical cues, the ECM-transmitted paratensile mechanical signaling can precisely guide the neuronal cells' migration and axon extension for synapse formation. The paratensile-signaling strategy can significantly raise up the precision and efficiency of the synaptic and neuronal system formation, especially in the complex microenvironment, in which the chemical cues alone might be easily disturbed. As a visco-elastic material, collagen fibers act as a bridge and transfer the tensile force signals precisely from one cell to the others.^[25] Because the width of the collagen fiber can reach to sub-micrometer scale, the spatial resolution for force signal transmission is much higher than that delivered by chemical signals. Thus, it can realize precise location to even the single axon.

It is also interesting to point out that the cyclic stretching force can guide the neuronal cells more efficiently than the static stretching on collagen ECM (Figure 5h,i). It is because that collagen ECM has properties of nonlinear visco-elasticity and stress relaxation.^[34] For collagen, immediately following the applied strain, the elastic modulus increased significantly over strain, while strain stiffening was substantially diminished within 1 s, and almost disappeared by 300 s, due to the strain-enhanced stress relaxation.^[34] Therefore, to maintain the tensile force sig-

nals, the deformation should be applied to the collagen repeatedly. Notably, the neuronal cells take the similar strategy to transmit signals, as we observed that the neuronal cells have innate rhythmic contraction with a time period of around 2–4 min, which is within the time range for collagen stress relaxation.^[34]

It is noteworthy that the reason of using quasi-3D system other than 3D system, in which cells are embedded in matrix, to analyze the paratensile signaling among neuronal cells is because quasi-3D system has less restriction for cell motility, providing an easier and better observing conditions. Meanwhile, we have also tested the neuronal cells embedded within 3D system, and the phenomenon presents the similar results as in quasi-3D system, but with shorter responding distance and weaker signals (Figure S6b, Supporting Information). As ECM in brain tissues contains not only collagen, but also many other softer components, such as hyaluronic acid (low molecular weight),^[52–53] it is more friendly for cell migration within the matrix of brain tissues, while maintaining functions for mechanical-signals transmission. In future, we need to further develop the ECM materials for in vitro brain model to reveal mechanism in more details.

Taken together, our results show that the precise neuronal cell pathfinding for synapse and neural networks formation can be guided by ECM-transmitted mechanical signals, which are then mechano-transduced into cells via calcium transients mediated by mechano-sensitive ion channels. This explains the important roles of abundant presented mechano-sensitive ion channels, such as Piezo 1, in neuronal cells.^[32,44] Also, this mechanism explains why the integration of fibrous hydrogels is essential in constructing in vitro models for regenerative medicine applications in the spinal cord.^[29] Thus, the novel matrix-transmitted mechanical signaling mechanism for synapse formation may open

a new window for neuron development studies and can provide guidelines for biomaterials designs in regenerative therapies for nervous system.

4. Experimental Section

Cell Culture and Sample Preparation: PC-12 cell line, one of the most used cell lines in neuroscience research, was obtained from China Infrastructure of Cell Line Resource. Mouse cerebral cortical neurons (Catalog # MIC-iCell-n005) were bought from iCell Bioscience Inc. The culture medium of PC-12 is RPMI-1640 (Gibco) supplemented with 10% fetal bovine serum (Gibco), 100 units mL⁻¹ penicillin, and 100 mg mL⁻¹ streptomycin (Gibco). The culture medium of mouse cerebral cortical neurons was brought from iCell Bioscience Inc.

Collagen I (Corning) solution was neutralized with 0.1 M NaOH to pH 7.4 and diluted to a final concentration of 2 mg mL⁻¹, then polymerized at 37 °C for 30 min to form a 3D hydrogel matrix with a thickness of around 1 mm. The cell suspension covered onto the matrix and stayed in the cell incubator for about 2 h for cell attaching and spreading before imaging. For cell migration tests and TFM analysis, cells were seeded sparsely (≈ 1 cell mm⁻²) on the collagen gel or culture dish. For cell self-organization tests, 2 mL of cell suspension with concentration of 5×10^4 cells mL⁻¹ covered on the collagen gel or culture dish. The actin polymerization inhibitor Latrunculin A, myosin II ATPase inhibitor Blebbistatin, integrin $\alpha 1\beta 1$ inhibitor Obtustatin, and mechanosensitive channels (Piezo and TRP families) inhibitor GsMTx4 was added to culture medium to treat cells 2 h after cells were seeded.

For cell on collagen under microflows experiment, flow was applied by simultaneously injecting and withdrawing cell culture medium at a flow rate of 60 $\mu\text{L h}^{-1}$ controlled by a syringe pump (Longer), on two counter sides of the chamber. For cell on collagen modified culture dish experiment, dilute collagen to 50 $\mu\text{g mL}^{-1}$ in 0.02 M acetic acid to the needed volume. Add diluted collagen, 5 $\mu\text{g cm}^{-2}$ surface area, to dish or plate, and incubate for 1 h at room temperature. Remove remaining collagen solution, and rinse dish 3 times with phosphate buffered saline (PBS) or culture medium.

Time-Lapse Imaging: Time-lapse images were obtained at 5 min intervals for 10 h using an inverted phase contrast microscope (Nikon Ti-E), equipped with an on-stage cell-culture incubator. Cell migration trajectories were abstracted by ImageJ (Manual Tracking plugin) and used for subsequent analysis of cell pair distance and cell migration characterization.

The dynamic processes of cell morphology and collagen fibers were visualized using laser scanning confocal microscope (LSCM, Leica SP8) with 25x water-immersion objective lens with NA of 0.95, lasting for 4–8 h at 0.5 h time interval. The collagen fiber microstructures are imaged in reflection mode of confocal microscopy. TFM analysis and calcium imaging data were also derived from images taken by confocal microscope, with time intervals shortened to 1 min and 10 s, respectively.

Statistical Analysis: The normalized cell distance was calculated using the equation, Normalized cell distance = CD_t/CD_0 , where CD_t is the distance between cell pair at time t , representing the changes of relative distance between cells with time.

Linearity was calculated using the equation, Linearity = $(CD_0 - CD_t)/(D_{1t} + D_{2t})$, where D_{1t} and D_{2t} are the lengths of migration trajectories of cell 1 and cell 2, respectively. This value represents the migration correlation between cells. If cells migrate directly towards each other, the value is approaching to 1.

The mean square displacement (MSD) of each trajectory was calculated using the equation, $MSD = \langle (d_t)^2 \rangle$, where the d_t is the straight-line distance between the start point of the trajectory and the current position at time t . The exponent α is determined using the nonlinear fitting of the points by $MSD = A \cdot t^\alpha$, which also corresponds to the slope of the MSD curve in the log–log plot. The α -value is a handy index for directional persistence: it equals to 1 for randomly moving cells and 2 for cells that move in a perfectly straight manner. If $1 < \alpha < 2$, the dynamics is super-diffusive, typically representing a mixing of ballistic and diffusive motion (such as persistent random walk).^[37]

Directional ratio refers to the ratio between the length from the start point to end point of the migration trajectory to the total length of trajectory. Directional ratio was calculated using the equation, Directional ratio = d_t/D_t , where the D_t is the actual length of trajectory between the start point and the current position, which is particularly affected by the instantaneous velocity of the cell. This ratio is equal to 1 for a straight cell trajectory and approaches to 0 for a highly curved trajectory.^[37]

The autocorrelation coefficient is the cosine of the angle (θ) between the displacement vectors of the two sequential steps (Figure 2h) and average the value of the cells at all times, Autocorrelation coefficient = $\langle \cos(\theta) \rangle = \langle (\mathbf{S}_{t-1} \cdot \mathbf{S}_t) / (|\mathbf{S}_{t-1}| |\mathbf{S}_t|) \rangle$, which has the advantage that it is not affected by velocity, but only measures direction changes of the trajectory.

Data are presented as median (center lines) of box (25th to 75th percentiles) and whisker (minimum to maximum) plots. Statistical significance of differences was tested using two-sample t -test ($*p < 0.05$, $**p < 0.01$, $***p < 0.001$). For the data of multiple groups of parallel experiments, error bar is expressed as Mean \pm SEM.

Cell Contraction Force Analysis: The cell force is analyzed with traction force microscopy (TFM). The microstructures of collagen fiber near cell were imaged by inverted microscope (Nikon Ti-E) with phase contrast mode or confocal microscope (Leica SP8) with reflection mode. As one of the TFM tracing algorithm, particle image velocimetry (PIV) is used to analyze the dynamic change of the ECM microstructures with Matlab program PIVlab. Thus, the deformation of collagen and divergence diagram can be further obtained.^[35–36] The size of PIV grid was set to 8 pixels and was shifted with an overlapping zone of 50%.

Divergence (θ) is computed from the deformation derivatives, $\theta = \partial u/\partial x + \partial v/\partial y$, and is insensitive to masking effects of high average deformation or background deformation, making it very useful in revealing the degree of collagen densification, which are not visible from the deformation map.^[35–36] In the system, the divergence indicates the rate of change in collagen volume, ignoring the vertical deformation of collagen. In simple terms, the collagen is compressed when the divergence is negative (red), and stretched when the divergence is positive (blue).

To calculate the average deformation of collagen over time, PIV results were oriented along the long axis of the cells ($\theta = 0^\circ$) with the cell centroid as the origin. The PIV data were segmented according to the distance to the cell centroid with an interval of 4 μm and the angle with an interval of 5° , and the mean value of each region was calculated to obtain the distribution of cell contraction force with distance and angle.

For the deformation of collagen along the long axis of cells over time, the cells were reoriented to be parallel to the image x -axis for imaging and PIV processing. The deformation component along the cell long axis (u component) was selected, and the average deformation along the long axis of cell was calculated, with a width of 20 μm transversal to long axis for averaging.

The normalized distance was calculated using the equation, Normalized distance = d_t/d_0 , where the d_0 and d_t are the initial and final distances from cell axon to micropipette tip, respectively.

Immunofluorescence Tests: Immunofluorescence tests were performed to examine protein expressions and cell morphological characteristics. Samples were fixed in prewarmed 4% paraformaldehyde (Sigma) and permeabilized in 0.5% Triton X-100 (Sigma), then incubated with primary Piezo1 polyclonal antibodies (PA5-106296, Invitrogen) and the following secondary antibodies Goat Anti-Rabbit IgG (H+L)-Alexa Fluor 488 (BN20635, Biorigin). Samples were also stained with TRITC Phalloidin (CA1610, Solarbio) and Hoechst (33 342, Invitrogen). All samples were treated with same procedures, and the imaging settings of confocal microscopy were also kept the same.

Physical Stretching on Collagen ECM: Cells were seeded onto 2 mg mL⁻¹ collagen gel and allowed to spread on the substrate for 2 h. The glass micropipette was controlled by a micromanipulator (InjectMan 4, Eppendorf) with customized moving trajectories control program (MATLAB). A force gradient was generated by inserting the micropipette into collagen gel at 100 μm away from the leading edge of the cell with an inserting angle of 30° – 60° , and then horizontally moving the micropipette away from the cell for 10 μm (Figure 5d–f). For cyclic stretching, collagen was pulled by the micropipette for 1 min and then released for 1 min

repeatedly, while in continuous stretching, the collagen was pulled for one time, without the releasing step. This method simulates the cell contraction process, allowing repeatedly achieving a consistent stimulation onto collagen in terms of position, duration, and force magnitude.

Stimulated cells were imaged at a 30 s time interval for ≈ 90 min by an inverted phase contrast microscope (Nikon Ti-E) with a 20x objective. To inhibit Piezo1 function, either 1 μM GsMTx4 or 1 mM EGTA (Sigma-Aldrich) was added to culture medium to treat cells 2 h before experiment.

Calcium Imaging and Analysis: Cells were loaded in medium with Calbryte-520 (5 μM , AAT) for 30 min at 37 °C and imaged on confocal microscope (25x) at 10 s interval for 1 h. The positions of the cell front were manually marked to calculate the axon extension speed. The dynamic states of protrusions are classified with their velocity (extending: velocity $> 0.1 \mu\text{m min}^{-1}$, stable: $-0.1 \mu\text{m min}^{-1} < \text{velocity} < 0.1 \mu\text{m min}^{-1}$, retracting: velocity $< -0.1 \mu\text{m min}^{-1}$). A $10 \mu\text{m} \times 10 \mu\text{m}$ area centered on the front of the axon was selected for calcium intensity data analysis. The averaged value of intensity was defined as F_0 , and the current intensity was F . When the F/F_0 value was large than 1.25, it was identified as a Ca^{2+} transient.

Supporting Information

Supporting Information is available from the Wiley Online Library or from the author.

Acknowledgements

The authors thanked Luru Dai and Yunqing Tang for assisting with apparatus. This work was supported by the National Key Research and Development Program of China (Grant No. 2020YFA0908200), the National Natural Science Foundation of China (NSFC) (Grant Nos. 12074407, 12090054, and T2221001), the Youth Innovation Promotion Association of CAS (Grant No. 2021007), the Strategic Priority Research Program of Chinese Academy of Sciences (Grant No. XDB33000000), and the Scientific Instrument Developing Project of the Chinese Academy of Sciences (Grant No. YJKYYQ20190034).

Conflict of Interest

The authors declare no conflict of interest.

Data Availability Statement

The data that support the findings of this study are available from the corresponding author upon reasonable request.

Keywords

axon pathfinding, extracellular matrix, mechanical signals, synapse formation

Received: February 19, 2023

Revised: April 11, 2023

Published online:

[1] J. N. Kay, *J. Cell Biol.* **2016**, *215*, 147.

[2] R. Ayala, T. Z. Shu, L. H. Tsai, *Cell* **2007**, *128*, 29.

[3] M. E. Williams, J. de Wit, A. Ghosh, *Neuron* **2010**, *68*, 9.

- [4] S. Batool, H. Raza, J. Zaidi, S. Riaz, S. Hasan, N. I. Syed, *J. Neurophysiol.* **2019**, *121*, 1381.
- [5] C. Ohtaka-Maruyama, M. Okamoto, K. Endo, M. Oshima, N. Kaneko, K. Yura, H. Okado, T. Miyata, N. Maeda, *Science* **2018**, *360*, 313.
- [6] T. C. Sudhof, *Neuron* **2018**, *100*, 276.
- [7] J. Q. Zheng, M. M. Poo, *Annu. Rev. Cell Dev. Biol.* **2007**, *23*, 375.
- [8] S. Yogev, K. Shen, *Neuron* **2017**, *96*, 638.
- [9] K. Franze, *Annu. Rev. Cell Dev. Biol.* **2020**, *36*, 61.
- [10] C. B. Guan, H. T. Xu, M. Jin, X. B. Yuan, M. M. Poo, *Cell* **2007**, *129*, 385.
- [11] T. M. Gomez, J. Q. Zheng, *Nat. Rev. Neurosci.* **2006**, *7*, 115.
- [12] P. A. Janmey, R. T. Miller, *J. Cell Sci.* **2011**, *124*, 9.
- [13] G. J. Goodhill, *Trends Neurosci.* **2016**, *39*, 202.
- [14] J. Seo, W. Youn, J. Y. Choi, H. Cho, H. Choi, C. Lanara, E. Stratakis, I. S. Choi, *Dev. Neurobiol.* **2020**, *80*, 361.
- [15] D. E. Koser, A. J. Thompson, S. K. Foster, A. Dwivedy, E. K. Pillai, G. K. Sheridan, H. Svoboda, M. Viana, L. D. Costa, J. Guck, C. E. Holt, K. Franze, *Nat. Neurosci.* **2016**, *19*, 1592.
- [16] M. Segel, B. Neumann, M. F. E. Hill, I. P. Weber, C. Viscomi, C. Zhao, A. Young, C. C. Agle, A. J. Thompson, G. A. Gonzalez, A. Sharma, S. Holmqvist, D. H. Rowitch, K. Franze, R. J. M. Franklin, K. J. Chalut, *Nature* **2019**, *573*, E3.
- [17] H. Ucar, S. Watanabe, J. Noguchi, Y. Morimoto, Y. Iino, S. Yagishita, N. Takahashi, H. Kasai, *Nature* **2021**, *600*, 686.
- [18] K. Franze, *Development* **2013**, *140*, 3069.
- [19] J. I. Puleo, S. S. Parker, M. R. Roman, A. W. Watson, K. R. Eliato, L. L. Peng, K. Saboda, D. J. Roe, R. Ros, F. B. Gertler, G. Mouneimne, *J. Cell Biol.* **2019**, *218*, 4215.
- [20] D. Shahriari, G. Loke, I. Tafel, S. Park, P. H. Chiang, Y. Fink, P. Anikeeva, *Adv. Mater.* **2019**, *31*, 1902021.
- [21] J. Jiang, Z. H. Zhang, X. B. Yuan, M. M. Poo, *J. Cell Biol.* **2015**, *209*, 759.
- [22] C. E. Chan, D. J. Odde, *Science* **2008**, *322*, 1687.
- [23] R. J. Polackwich, D. Koch, R. McAllister, H. M. Geller, J. S. Urbach, *Front. Cell Neurosci.* **2015**, *9*, 417.
- [24] J. W. Yuan, Y. N. Zhang, Y. R. Liu, W. Li, S. X. Dou, Y. Wei, P. Y. Wang, H. Li, *Small* **2022**, *18*, 2106498.
- [25] Q. H. Fan, Y. Zheng, X. C. Wang, R. P. Xie, Y. Ding, B. Y. Wang, X. Y. Yu, Y. Lu, L. Y. Liu, Y. L. Li, M. Li, Y. J. Zhao, Y. Jiao, F. F. Ye, *Angew. Chem., Int. Ed.* **2021**, *60*, 11858.
- [26] L. W. Liu, H. S. Yu, H. Zhao, Z. Z. Wu, Y. Long, J. B. Zhang, X. J. Yan, Z. F. You, L. Zhou, T. Xia, Y. Shi, B. L. Xiao, Y. X. Wang, C. Y. Huang, Y. N. Du, *Proc. Natl. Acad. Sci. USA* **2020**, *117*, 10832.
- [27] S. Usmani, E. R. Aurand, M. Medelin, A. Fabbro, D. Scaini, J. Laishram, F. B. Rosselli, A. Ansuini, D. Zoccolan, M. Scarselli, M. De Crescenzi, S. Bosi, M. Prato, L. Ballerini, *Sci. Adv.* **2016**, *2*, e1600087.
- [28] D. Joung, N. S. Lavoie, S. Z. Guo, S. H. Park, A. M. Parr, M. C. McAlpine, *Adv. Funct. Mater.* **2020**, *30*, 1906237.
- [29] J. Koffler, W. Zhu, X. Qu, O. Platoshyn, J. N. Dulin, J. Brock, L. Graham, P. Lu, J. Sakamoto, M. Marsala, S. C. Chen, M. H. Tuszynski, *Nat. Med.* **2019**, *25*, 263.
- [30] J. Kim, C. A. Jones, N. S. Groves, B. Sun, *PLoS One* **2016**, *11*, e0156797.
- [31] J. Steinwachs, C. Metzner, K. Skodzek, N. Lang, I. Thievensen, C. Mark, S. Munster, K. E. Aifantis, B. Fabry, *Nat. Methods* **2016**, *13*, 171.
- [32] F. Li, T. Y. Lo, L. Miles, Q. Wang, H. N. Noristani, D. Li, J. Niu, S. Trombley, J. I. Goldshteyn, C. Wang, S. Wang, J. Qiu, K. Pogoda, K. Mandal, M. Brewster, P. Rompolas, Y. He, P. A. Janmey, G. M. Thomas, S. Li, Y. Song, *Nat. Commun.* **2021**, *12*, 3845.
- [33] Z. Alvarez, A. N. Kolberg-Edelbrock, I. R. Sasselli, J. A. Ortega, R. Qiu, Z. Syrgiannis, P. A. Mirau, F. Chen, S. M. Chin, S. Weigand, E. Kiskinis, S. I. Stupp, *Science* **2021**, *374*, 848.

- [34] S. Nam, K. H. Hu, M. J. Butte, O. Chaudhuri, *Proc. Natl. Acad. Sci. USA* **2016**, *113*, 5492.
- [35] E. J. Stamhuis, *Aquat. Ecol.* **2006**, *40*, 463.
- [36] W. Thielicke, R. Sonntag, *J. Open Res. Softw.* **2021**, *9*, 12.
- [37] R. Gorelik, A. Gautreau, *Nat. Protoc.* **2014**, *9*, 1931.
- [38] Y. F. Huang, G. Gompper, B. Sabass, *Comput. Phys. Commun.* **2020**, *256*, 107313.
- [39] C. M. Lo, H. B. Wang, M. Dembo, Y. L. Wang, *Biophys. J.* **2000**, *79*, 144.
- [40] K. Franze, J. Gerdemann, M. Weick, T. Betz, S. Pawlizak, M. Lakadamyali, J. Bayer, K. Rillich, M. Gogler, Y. B. Lu, A. Reichenbach, P. Janmey, J. Kas, *Biophys. J.* **2009**, *97*, 1883.
- [41] V. Raffa, F. Falcone, S. De Vincentiis, A. Falconieri, M. P. Calatayud, G. F. Goya, A. Cuschieri, *Biophys. J.* **2018**, *115*, 2026.
- [42] Y. L. Han, P. Ronceray, G. Xu, A. Malandrino, R. D. Kamm, M. Lenz, C. P. Broedersz, M. Guo, *Proc. Natl. Acad. Sci. USA* **2018**, *115*, 4075.
- [43] I. Nitsan, S. Drori, Y. E. Lewis, S. Cohen, S. Tzlil, *Nat. Phys.* **2016**, *12*, 472.
- [44] M. M. Pathak, J. L. Nourse, T. Tran, J. Hwe, J. Arulmoli, D. T. T. Le, E. Bernardis, L. A. Flanagan, F. Tombola, *Proc. Natl. Acad. Sci. USA* **2014**, *111*, 16148.
- [45] Y. Y. Wang, H. Zhang, T. Ma, Y. Lu, H. Y. Xie, W. Wang, Y. H. Ma, G. H. Li, Y. W. Li, *Biochem. Biophys. Res. Commun.* **2019**, *513*, 147.
- [46] S. Sugio, M. Nagasawa, I. Kojima, Y. Ishizaki, K. Shibasaki, *FASEB J.* **2017**, *31*, 1368.
- [47] S. Yoo, D. R. Mittelstein, R. Hurt, J. Lacroix, M. G. Shapiro, *Nat. Commun.* **2022**, *13*, 493.
- [48] T. T. Liu, X. F. Du, B. B. Zhang, H. X. Zi, Y. Yan, J. A. Yin, H. Hou, S. Y. Gu, Q. Chen, J. L. Du, *Neuron* **2020**, *108*, 180.
- [49] H. Komuro, T. Kumada, *Cell Calcium*. **2005**, *37*, 387.
- [50] T. M. Gomez, N. C. Spitzer, *Nature* **1999**, *397*, 350.
- [51] M. J. Berridge, P. Lipp, M. D. Bootman, *Nat. Rev. Mol. Cell Biol.* **2000**, *1*, 11.
- [52] K. Franze, P. A. Janmey, J. Guck, *Annu. Rev. Biomed. Eng.* **2013**, *15*, 227.
- [53] J. M. Barnes, L. Przybyla, V. M. Weaver, *J. Cell Sci.* **2017**, *130*, 71.